A THEORY FOR LOW-GRAVITY FUEL SLOSHING IN AN ARBITRARY AXISYMMETRIC RIGID TANK

by

WEN-HWA CHU

ASME PAPER 70-APM-EEE, to be published in *Transactions ASME, Journal of Applied Mechanics*

NOTE: The numerical examples in the published paper contain several errors. For that reason, the original examples have been corrected for this report and appear here as Appendix D to the paper.

Introduction

THE behavior and consequences of fuel sloshing in rockets under a high effective gravity were recognized problems which have been quite well understood [1–3].[1] The problem of low-gravity fuel sloshing, characterized by the significant role of interfacial tension, is now a subject of importance for application to coasting rockets or orbital stations.

The equilibrium behavior of fluids at zero and/or low gravity has been studied in references [4–7]. The theoretical determination of an equilibrium interface shape is nonlinear and requires a trial and error procedure for a given contact angle [5, 6].

Satterlee and Reynolds [8] have successfully solved the free sloshing problem in cylindrical containers under low gravity and formulated a variational principle for this purpose. Yeh [9], using a similar approach, solved the free and forced sloshing problem under low-gravity conditions, without force and moment or an equivalent mechanical model. Dodge and Garza [10, 11] performed force measurements under simulated low-gravity conditions and predicted forces and moment for circular cylindrical tanks under lateral (translational) motion. The equivalent spring-mass model was given in [10]. Additional work by Dodge and Garza for other special tanks was given in [12, 13]. A finite-difference approach with application to a hemispherically bottomed cylindrical tank and spheroidal tanks was given by Concus, Crane, and Satterlee in [14, 15].

These investigations indicate a need of a program for a general axisymmetric tank. A preliminary study on liquid sloshing in an arbitrary axisymmetric tank was reported in [16], but it is limited to translational oscillations. It is the object of the present paper to present a seminumerical approach for an arbitrary axisymmetric tank with simplified force and moment calculations and the resultant mechanical model for both pitching and translational oscillations. A general computer program utilizing Winslow method [17] will be completed to obtain sloshing frequencies, slosh mass, and mass-height, for which a brief description is given in Appendix A.

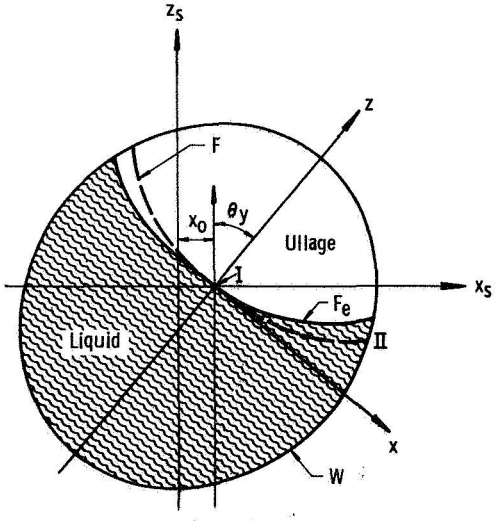

Fig. 1 Some Nomenclatures

[1] Numbers in brackets designate References at end of paper.

Contributed by the Applied Mechanics Division for publication (without presentation) in the JOURNAL OF APPLIED MECHANICS.

Governing Equations

Assuming irrotational incompressible flow, there is a space-fixed velocity potential[2] ϕ satisfying the Laplace equation in both space-fixed and tank-fixed coordinates

$$\nabla_s^2\phi = 0,\ \nabla^2\phi = 0;$$

$$\nabla_s^2 = \frac{\partial^2}{\partial x_s^2} + \frac{\partial^2}{\partial y_s^2} + \frac{\partial^2}{\partial z_s^2},\ \nabla^2 = \frac{\partial^2}{\partial x^2} + \frac{\partial^2}{\partial y^2} + \frac{\partial^2}{\partial z^2} \quad (1)$$

As in thin airfoil theory, the velocity potential can be obtained by imposing boundary conditions on the initial or mean position, but the hydrostatic pressure due to gravity possesses components along both the tank axis z and the lateral axis x, Fig. 1, for pitching oscillations. The linearized Bernoulli's equation states

$$p - p_I + \rho\frac{\partial\phi}{\partial t} + \rho g(z - x\theta_y) = 0 \quad (2)[3]$$

and

$$p - p_{uI} + \rho_u\frac{\partial\phi_u}{\partial t} + \rho_u g(z - x\theta_y) = 0 \quad (3)$$

for the liquid and the ullage, respectively, and p_I, p_{uI} are constants.

Boundary Conditions

The linearized interface kinematic condition states that

$$\frac{\partial h}{\partial t} \cong \frac{\partial\phi}{\partial n} \quad \text{on } F \quad (4)[4]$$

The interface dynamic condition states that

$$-p_- + p_+ = \sigma\kappa = \sigma\kappa_0 + \sigma\kappa' \quad \text{on } F_e \quad (5)$$

For the "mean" interface location f (in general, $p_I = p_I^\circ + p_I'$, p_I°, p_I' being constants),

$$-\sigma\kappa_0 + (\rho - \rho_u)gf - (p_I^\circ - p_{uI}^\circ) = 0 \quad \text{on } F \quad (6)$$

where the curvature of the mean interface, κ_0, is axisymmetric and

$$\kappa_0 = \frac{1}{r}\frac{\partial}{\partial r}\left\{\frac{r\dfrac{\partial f}{\partial r}}{\sqrt{1 + \left(\dfrac{\partial f}{\partial r}\right)^2}}\right\} = \frac{1}{r}\frac{\partial f}{\partial s} + \left(\frac{\partial r}{\partial s}\frac{\partial^2 f}{\partial s^2} - \frac{\partial f}{\partial s}\frac{\partial^2 r}{\partial s^2}\right) \quad (6a)$$

Equation (6) holds for $r = 0$, thus

$$p_I^\circ - p_{uI}^\circ = -2\left(\frac{\partial^2 f}{\partial r^2}\right)_{II}$$

The linearized interface dynamic condition is then

$$-(p_u' - p_{uI}') - \sigma\kappa' + \rho\frac{\partial\phi}{\partial t} - \rho_u\frac{\partial\phi_u}{\partial t} + (\rho - \rho_u)gh\frac{\partial r}{\partial s} - (\rho - \rho_u)gx\theta_y = 0 \quad (7)[5]$$

[2] For example, $\partial\phi/\partial x$ gives velocity component in x-direction with respect to space-fixed coordinates.

[3] Chu, W. H., "Free Surface Condition for Sloshing Resulting From Pitching and Some Corrections," *ARS Journal*, Vol. 30, Nov. 1960, pp. 1093–1094.

[4] A vertical interface description was used but is only successful when $(dF/dR)^{-1}$ does not vanish on the interface.

[5] For sinusoidal oscillations and $m = 1$, $h = 0$, $\phi = \phi_u = 0$, $x = 0$, and $\kappa' = 0$ at point I, thus $p_I' - p_{uI}' = 0$. For other m values, $-p_I' + p_{uI}^\circ = \sigma\kappa_I'$, which will be omitted until needed.

where the perturbation curvature for cos $(m\theta)$ variation is to the first order

$$\kappa' = \frac{\partial^2 h}{\partial \mathbf{s}^2} + \frac{1}{r}\frac{\partial r}{\partial \mathbf{s}}\frac{\partial h}{\partial \mathbf{s}} + \frac{1}{r^2}\frac{\partial^2 h}{\partial \theta^2} + \left[\left(\frac{1}{r}\frac{\partial f}{\partial \mathbf{s}}\right)^2 + \left(\frac{\partial r}{\partial \mathbf{s}}\frac{\partial^2 f}{\partial \mathbf{s}^2} - \frac{\partial f}{\partial \mathbf{s}}\frac{\partial^2 r}{\partial \mathbf{s}^2}\right)^2\right] h \quad (7a)^6$$

m being unity for lateral excitation of a rigid tank. At point I, the origin, $h = 0$, $\phi = 0$, $\kappa' = 0$, and thus $p_I = p_{uI}$. For most analyses, $\rho_u = 0$ was assumed. We shall assume the impulsive pressure in the ullage is negligible, i.e., $\phi_u = 0$. Then, for sinusoidal oscillations with h, ϕ proportional to cos (ωt) and sin (ωt), respectively, equations (7), (7a), and (4) yield

$$-\left\{\frac{1}{R}\frac{\partial}{\partial s}\left(R\frac{\partial H}{\partial s}\right) - \frac{m^2}{R^2}H + GH\right\} + N_{B_e}H\frac{\partial R}{\partial s} + \theta_y N_{B_e} R\cos\theta + \Omega^2\Phi = 0 \quad \text{on } F \quad (7b)^7$$

where

$$G = \left(\frac{1}{R}\frac{\partial F}{\partial s}\right)^2 + \left(\frac{\partial R}{\partial s}\frac{\partial^2 F}{\partial s^2} - \frac{\partial F}{\partial s}\frac{\partial^2 R}{\partial s^2}\right)^2 = \frac{1}{R^2}\frac{{F_R}^2}{(1+{F_R}^2)} + \left[\frac{F_{RR}}{(1+{F_R}^2)^{3/2}}\right]^2 \quad (7c)$$

It is noted that, for lateral oscillations, $m = 1$, solutions are proportional to cos θ.

The boundary condition on the wall is that the relative normal velocity be zero, i.e., with cos $(n, x) = \dfrac{\partial x}{\partial n}$ and cos $(n, z) = \dfrac{\partial z}{\partial n}$,

$$\frac{\partial \phi}{\partial n} = \dot{x}_0\frac{\partial x}{\partial n} \quad (8)$$

and

$$\frac{\partial \phi}{\partial n} = \dot{\theta}_y\left(z\frac{\partial x}{\partial n} - x\frac{\partial z}{\partial n}\right) \quad (9)$$

for translational and pitching oscillations, respectively.

In addition, there is an interface contact point condition which takes the form [8, 9, and 15]

[6] The instantaneous interface can be described by the position vector $\mathbf{r}/a = [R - HF_s]\cos\theta\hat{i} + [R - HF_s]\sin\theta\hat{j} + [F + HR_s]\hat{k}$; $R_s = dR/ds$, $F_s = dR/ds$. The curvatures can then be derived from the fundamental magnitudes [18] neglecting higher-order terms. The linearized total curvature is given by this equation, which was first derived in [15] by a different procedure.

[7] For sinusoidal oscillations, without loss of generality, $\dot{x}_0$, θ_y, ϕ are assumed to be proportional to sin (ωt) while h is proportional to cos (ωt).

Nomenclature

a = reference length, say, maximum radius of tank
$d\mathbf{A}$ = dA/a^2 (a scalar)
dA = $rdrd\theta$
$d\mathbf{S}$ = dS/a^2, nondimensional surface element (a scalar)
dS = 3-D surface element, e.g., $rd\theta d\mathbf{s}$
F = equilibrium (mean) interface of f/a
F_e = instantaneous interface
F_H = horizontal force defined by equation (19)
F_R = (dF/dR), slope of F in the generatrix plane
F_x = x-component of force on tank
f = equilibrium (mean) interface elevation measured along vertical axis
g = gravitational acceleration
H = amplitude of h/a, nondimensional slosh height
h = interface perturbation normal to equilibrium interface
h_0 = reference length, say, depth of liquid at center of tank
M_0, I_0 = rigid mass and moment of inertia of mechanical model
M_F = liquid mass
M_y = pitching moment about y-axis
m_k = kth slosh mass
N_B = Bond number, $\rho a^2 g/\sigma$
n = outer normal
n_0 = n/a, nondimensional normal distance
p = pressure
p_I = equilibrium liquid pressure at origin—a constant
p_u = ullage pressure
p_{uI} = equilibrium ullage pressure at origin—a constant
R = r/a, nondimensional radius
r, θ, z = tank fixed cylindrical coordinates
s = arc length nondimensionalized by a
$\mathbf{s}$ = arc length (a scalar)
t = time
V = volume of liquid divided by a^3
V_L = liquid volume
W = wall wetted by liquid
W_e = instantaneous wetted wall below instantaneous interface, F_e
x_0 = translational amplitude in x_s-direction
x_s, y_s, z_s = space-fixed rectangular coordinates
Γ = γa, nondimensional contact point constant
γ = hysteresis coefficient or contact point constant
$\Delta\rho$ = density difference, $\rho - \rho_u$
δ_{ij} = Kronecker delta
ϵ_1 = sign of $n\cdot\hat{z}$, cos (n, z), or $\partial z/\partial n$
θ_y = amplitude of pitching about y-axis
κ = mean curvature
κ' = perturbation of mean curvature
λ_j = jth eigenvalue $(m = 1)$
λ_{mj} = jth eigenvalue corresponds to mth circumferential mode
ρ = liquid density
ρ_u = density of ullage fluid (vapor or gas)
σ = surface tension
Φ = amplitude of nondimensional velocity potential, $\phi/\omega a^2$
Φ_k = amplitude of nondimensional potential $\phi_k/\omega a^2$
Φ_N = see equation (15)
Φ° = amplitude of nondimensional potential $\phi^\circ/\omega a^2$
ϕ = velocity potential
ϕ_k = velocity potential of the kth natural mode
ϕ' = additional velocity potential due to interface movement
ϕ° = velocity potential of liquid with a frozen interface
ψ = velocity potential of auxiliary eigenfunctions
ψ_j = jth auxiliary characteristic function
Ω^2 = $\rho a^3\omega^2/\sigma$; product of Bond number, $\rho a^2 g/\sigma$, and frequency parameter, $\omega^2 a/g$
ω = frequency of oscillation
ω_k = kth natural frequency

Subscripts

$(\ )_I$ = $(\ )$ at vertex of equilibrium interface (origin)
$(\ )_{II}$ = $(\ )$ at contact point in generatrix plane
$(\ )_{CG}$ = $(\ )$ related to center of gravity
$(\ )_e$ = effective value of $(\ )$
$(\ )_F$ = $(\ )$ on F
$(\ )_m$ = $(\ )$ associated with cos $(m\theta)$ mode
$(\ )_p$ = $(\ )$ related to pitching
$(\ )_T$ = $(\ )$ related to translation
$(\ )_W$ = $(\ )$ on W
$(\ )_u$ = $(\ )$ related to ullage
$(\ )_-$ = $(\ )$ just below interface
$(\ )_+$ = $(\ )$ just above interface

$$\frac{\partial h}{\partial \mathbf{s}} = \gamma h \quad \text{or} \quad \frac{\partial H}{\partial s} = \Gamma H \quad \text{at point II} \tag{10}$$

where γ may be a frequency-dependent constant. However, if the contact angle remains constant, we can show that (see Appendix C[8])

$$\gamma = +\frac{1}{\sin\theta_c}\left\{\left|\frac{z_{rr}}{(1+z_r^2)^{3/2}}\right|_{W,\mathrm{II}} - \cos\theta_c \left|\frac{f_{rr}}{(1+f_r^2)^{3/2}}\right|_{\mathrm{II}}\right\} \tag{10a}$$[9]

$$\Gamma = \gamma a \tag{10b}$$

where

$$z_r = \frac{dz}{dr}, f_r = \frac{df}{dr}, z_{rr} = \frac{d^2z}{dr^2}, f_{rr} = \frac{d^2f}{dr^2}; \quad z \text{ on } W, f \text{ on } F$$

Method of Solution

We shall decompose ϕ into two parts, ϕ' and ϕ°: ϕ° is the velocity potential corresponding to a liquid contained by a rigid mean interface and the tank walls. Therefore, it satisfies the Laplace equation and the nonhomogeneous boundary condition on the contour, equation (8) for translation and equation (9) for pitching on F_e and W_e. It is noted that

$$\phi_T{}^0 = \dot{x}_0 x \tag{11}$$

while $\phi_p{}^\circ$ can be constructed numerically.

ϕ' is the perturbed velocity potential due to sloshing which is governed by the Laplace equation, the zero normal velocity condition at the wall and the resultant interface condition. The first two are satisfied by expansion in normal modes and the last by equations (15) and (16). In this paper, the normal modes are determined by expansion into a set of auxiliary characteristic functions[10] ψ_j, which is orthogonal on the curved interface, and satisfies the Laplace equation and the zero normal velocity wall condition.[11] The interface condition governing normal modes is second order [see equation (7b)] subject to zero H at center and the contact point condition, equation (10a) at wall. The former is satisfied as ψ_j vanishes along tank center line. The interface equation is approximately satisfied by a modified Galerkin method (the strict Galerkin method is given in [19]), which is illustrated in Appendix B. In this method, the contact point condition was imposed on the whole series, not term by term. The numerical results shown later substantiate the method used.

The force and moment are obtained by integration of pressure, not only on the wall, but also on the interface since the direct surface tension force and moment on the tank is equivalent to those on the interface due to pressure, assuming the interface inertia is negligible, as well as the interface mass. To put results in the mechanical model form, the divergence theorem has been most useful (with some manipulations).

Analytical Results

Free Oscillations. For free oscillations, the natural mode ϕ_k is expanded into a truncated series of the auxiliary eigenfunctions, i.e.,

$$\Phi_k = \frac{\phi_k}{\omega a^2} = \sum_{j=1}^{j_{mx}} c_{kj}\psi_{m_j}\cos(m\theta),\ \psi_j = \psi_{m_j}\cos(m\theta) \tag{12a, b}$$

$$H_k = \frac{h_k}{a} = -\sum_{j=1}^{J_{mx}} c_{kj}\psi_{m_j}\cos(m\theta) \tag{12c}$$

c_{kj} is the kth eigenvector of the following matrix equation obtained by a modified Galerkin method (Appendix B) from integrating the nondomensional equation (7b) with $\theta_y = 0$ and weighting function $\psi_{m_i} dS/\alpha_{m_i}{}^2$:

$$\left\{-\Gamma[\nu_{m_{ij}}] + [\gamma_{m_{ij}}] + m^2[\epsilon_{m_{ij}}] + \frac{\Delta\rho}{\rho}N_B[\beta_{m_{ij}}] - \Omega^2[\Delta_{m_{ij}}]\right\}\{c_j\} = 0;\ i, j = 1 \text{ to } J_{mx} \tag{13}$$

where

$$\beta_{m_{ij}} = \frac{\lambda_{m_{ij}}}{\alpha_{m_i}{}^2}\int_F \frac{\psi_{m_i}\psi_{m_j}\epsilon_1}{\sqrt{1+F_R{}^2}}\,dS,\ \epsilon_1 = \mathrm{sgn}\left(\frac{\partial R}{\partial s}\right) \tag{13a}$$[12]

$$\epsilon_{m_{ij}} = \frac{\lambda_{m_j}}{\alpha^2{}_{m_i}}\int_F \frac{1}{R^2}\psi_{m_i}\psi_{m_j}dS \tag{13b}$$

$$\nu_{m_i} = \frac{2\pi\lambda_{m_{ij}}}{\alpha_{m_i}{}^2}[R\psi_{m_i}\psi_{m_j}] \tag{13c}$$

$$\gamma_{m_{ij}} = \frac{\lambda_{m_j}}{\alpha_{m_i}{}^2}\left\{\int_F [1+F_R{}^2]^{-1}\frac{d\psi_{m_i}}{dR}\frac{d\psi_{m_j}}{dR}\,dS - \int_F G\psi_{m_i}\psi_{m_j}\,dS\right\} \tag{13d}$$

$$\Delta_{m_{ij}} = \frac{1}{\alpha_{m_i}{}^2}\int_F \psi_{m_i}\psi_{m_j}\,dS = \delta_{ij} \tag{13e}$$

$$\alpha_{m_i}{}^2 = \int_F \psi_{m_i}{}^2\,dS \tag{13f}$$

and $m = 1$ for lateral excitation of a rigid tank.

Forced Oscillations. Let

$$\phi' = -\omega a^2\sum_{k=1}^{K_{mx}} d_k\Phi_k;\ d_k = \frac{\bar{d}_k\Omega^2}{\Omega_k{}^2 - \Omega^2};\ \Phi_k = \sum_{j=1}^{J_{mx}} c_{kj}\psi_j \tag{14a, b, c}$$

in order to satisfy the interface condition that

$$\sum_{k=1}^{K_{mx}} d_k(\Omega_k{}^2 - \Omega^2)\Phi_k = -\Omega^2\Phi^\circ + \epsilon_2 N_B\frac{\Delta\rho}{\rho}\frac{x}{a}\theta_y \equiv \Phi_N\Omega^2 \tag{15}$$

$\epsilon_2 = 0$ for translational oscillation, $\epsilon_2 = 1$ for pitching oscillation. We have by the Galerkin procedure [19, equation (115.5), p. 435]

$$\sum_{k=1}^{K_{mx}} \bar{d}_k\int_F \Phi_k(-H_l)dS = \int_F \Phi_N(-H_l)dS,\ l = 1 \text{ to } K_{mx} \tag{16}$$

A weighting function of H_l was used taking advantage of the biorthogonal relation, equation (17). This assures the first K_{mx} components of the error as series in ϕ_k be zero. $\bar{d}_k$ can be solved from equation (16) by matrix inversion. There is no need of storing information of ψ_j inside the fluid domain as only the force and moment are of interest. It is noted in the limit [8 and 9]

$$\int_F \Phi_k(-H_l)dS = \delta_{kl}\int_F \Phi_k(-H_k)dS \tag{17}$$[13]

[8] Appendix is not in order of mention.

[9] An equivalent form was first derived in reference [15].

[10] For direct application of the Winslow method [17], we impose the simpler normal derivation condition, $\partial\psi_j/\partial n_0 = \lambda\psi_j$, on F and used the well-known influence coefficient technique to determine the eigenvector ψ_j on the intersurface, the eigenvalue λ_j.

[11] Strictly speaking, the boundary conditions are imposed in Winslow method, while the solution not proven to satisfy these conditions is correct on physical grounds (see Appendix A).

[12] The orthogonality property of ψ_j, thus, ψ_{m_j}, can be easily proved [16] as in the high-G case. $\cos^2(m\theta)$ in the integrand are uniformly omitted as they contribute the same factor, 1/2.

[13] This is referred to as biorthogonal relation.

then,

$$\bar{d}_l = \frac{\int_F \Phi_N(-H_l)dS}{\int_F \Phi_l(-H_l)dS} \tag{18}$$

which was utilized in proving that a unique spring-mass system exists for both pitching and translation.

Force and Moment. The force and moment exerted by a spring-mass system, Fig. 2, without damping were written in the following form [20] and remain valid if contributions due to direct surface tension are included

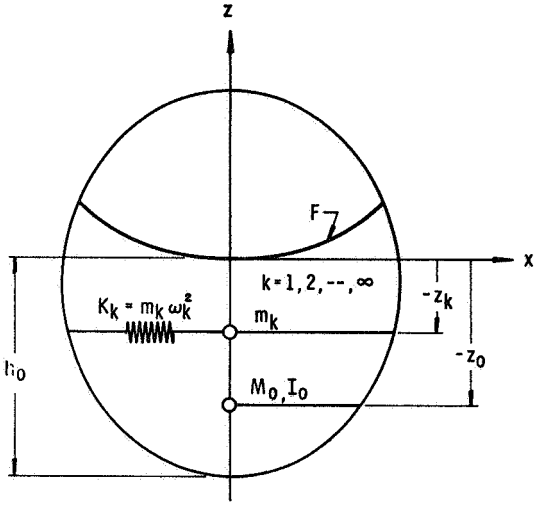

Fig. 2 Equivalent mechanical model

$$F_H = F_x - M_F g\theta_y \tag{19}$$

$$F_{H_T} = x_0\omega^2 M_F \left\{1 + \sum_{k=1}^{\infty} \frac{m_k}{M_F} \frac{1}{\left(\frac{\omega_k^2}{\omega^2} - 1\right)}\right\} \tag{20}$$

$$M_{y_T} = x_0\omega^2 M_F h_0 \left\{\frac{z_{CG}}{h_0} + \sum_{k=1}^{\infty} \frac{m_k}{M_F}\left(\frac{z_k}{h_0} + \frac{g}{h_0\omega^2}\right) \frac{1}{\left(\frac{\omega_k^2}{\omega^2} - 1\right)}\right\} \tag{21}$$

$$F_{H_p} = \theta_y\omega^2 M_F h_0 \left\{\frac{z_{CG}}{h_0} + \sum_{k=1}^{\infty} \frac{m_k}{M_F}\left(\frac{z_k}{h_0} + \frac{g}{h_0\omega^2}\right) \frac{1}{\left(\frac{\omega_k^2}{\omega^2} - 1\right)}\right\} \tag{22}$$

$$M_{y_p} = \theta_y\omega^2 M_F h_0^2 \left\{\frac{I_F}{M_F h_0^2} + \sum_{k=1}^{\infty} \frac{m_k}{M_F}\left(\frac{z_k}{h_0} + \frac{g}{\omega^2 h_0}\right)^2 \frac{1}{\left(\frac{\omega_k^2}{\omega^2} - 1\right)}\right\} + \theta_y g M_F h_0 \left(\frac{z_{CG}}{h_0}\right) \tag{23}$$

with rigid mass m_0, its location z_0, and moment of inertia I_0 given by

$$\frac{m_0}{M_F} = 1 - \sum_{k=1}^{\infty} \frac{m_k}{M_F} \tag{24}$$

$$\frac{z_0}{h_0} = \frac{1}{\frac{m_0}{M_F}}\left[\frac{z_{CG}}{h_0} - \sum_{k=1}^{\infty} \frac{z_k}{h_0}\frac{m_k}{M_F}\right] \tag{25}$$

$$\frac{I_0}{M_F h_0^2} = \frac{I_F}{M_F h_0^2} - \left(\frac{m_0}{M_F}\frac{z_0^2}{h_0^2} + \sum_{k=1}^{\infty} \frac{m_k}{M_F}\frac{z_k^2}{h_0^2}\right) \tag{26}$$

The force due to liquid pressure and direct surface tension is

$$F_x = \int_{W_e+F_e} p\,\frac{\partial x}{\partial n}\,dS \tag{27}$$[14]

and the moment due to liquid pressure and direct surface tension is

$$M_y = \int_{W_e+F_e} p\left(z\,\frac{\partial x}{\partial n} - x\,\frac{\partial z}{\partial n}\right) dS \tag{28}$$

it can be shown that

$$\frac{m_k}{M_F} = \bar{d}_{kT} f_k' \frac{1}{V} \tag{29}$$

where

$$f_k' = \sum_{j=1}^{\infty} c_{kj} \int_F \lambda_j \psi_j \frac{x}{a}\,d\mathbf{S} \tag{29a}$$

$$\bar{d}_{kT} = \frac{1}{\beta_k^2}\int_{W+F} \Phi_k \frac{\partial x}{\partial n}\,d\mathbf{S} \cong \frac{1}{\beta_k^2}\sum_{j=1}^{J_{mx}} c_{kj}\lambda_j \int_F \frac{x}{a}\psi_j\,d\mathbf{S} \tag{29b}$$[15]

$$V = V_L/\rho a^3,\ \beta_k^2 = \int_F \Phi_k(-H_k)d\mathbf{A} \tag{29c, d}$$

and

$$\frac{z_k}{a} = \frac{1}{\frac{m_k}{M_F}}\left(\frac{l_k'}{V}\right) \tag{30}$$

where

$$l_k' = \bar{d}_{kT}\sum_{j=1}^{\infty} c_{kj}\mu_j \tag{30a}$$

$$\mu_j = \int_{F+W} \psi_j \left(\frac{z}{a}\frac{\partial x}{\partial n} - \frac{x}{a}\frac{\partial z}{\partial n}\right) d\mathbf{S} \tag{30b}$$

and that

$$I_F = M_F a^2 I_F^*,\ I_F^* \cong \frac{1}{V}\int_{W+F} \Phi_p{}^{\circ} \left(\frac{z}{a}\frac{\partial r}{\partial n} - \frac{x}{a}\frac{\partial z}{\partial n}\right) d\mathbf{S} \tag{31a, b}$$

In deriving the mechanical model, ρ_u has been set to zero. A simple modification can be made for small ullage density by using

$$N_{B_e} = \frac{\Delta\rho}{\rho} N_B$$

the effective Bond number instead of the Bond number based on the density of the liquid, provided that the dynamic pressure due

[14] It is important to note that great simplification in results, when reduced to the mechanical model for both translation and pitching, is achieved by consideration of balance of forces acting on the thin interface as a free body. The force and moment on the tank due to direct surface tension must be equal to those acting on the interface by liquid pressure. These were not included in reference [15].

[15] For finite J_{mx}, it was found that $\bar{d}_{kT}$, determined by matrix inversion of equation (16) without using biorthogonal relation, yields results in better agreement with Dodge's theory [12] than equation (29b) which is correct in the limit.

to ullage motion is negligible.

It is noted that to prove the mechanical model for pitching motion frequent application of divergence theorem combined with differential properties of the auxiliary characteristic functions and the coordinate functions x and z were used. For brevity, the details are not included in this paper.

Numerical Examples. The present computer program has been checked out for several examples in Appendix III. These include cylindrical tanks, spherical tanks, and spheroidal tanks. Good agreement of first spring-mass with known theory or experiments was obtained with as few as 11 or 12 interface net points and the first seven auxiliary characteristic functions. Finer nets may yield higher accuracies, especially for the higher modes.

Machine Time. For a 12 × 18 mesh and a 12 × 12 mesh, the CDC-6600 central process time is a little over 2 min, while for the 23 × 34 mesh it is about 21 min. Most of the computing time was expended for the generation of influence coefficients, each of which is a Neumann problem. However, the influence coefficient method may be more convenient than the inversion of a large matrix, if not faster. No computer running time was reported in references [14 and 15], which finds natural modes by finite-differences and (partial) matrix inversion.

Conclusion

It seems that the present method yielded a practical way of computing the fundamental natural frequency, the first slosh mass, and its location. Higher masses and locations are usually not needed for design purposes and can be obtained by using finer meshes and longer machine time. A computer program utilizing triangular meshes and Winslow method [17] has been successfully employed and is expected to be completed in the near future for the titled problem. However, the present logical diagram may be limited to a convex axisymmetric tank for good accuracy.

Acknowledgments

The author would like to take this opportunity to thank D. R. Saathoff, A. F. Mueller, and R. Gonzales for writing the computer programs, and Dr. Franklin T. Dodge for his helpful discussions. The present research is supported by NASA Contract NAS8-20290, George C. Marshall Space Flight Center.

References

1 Abramson, H. N., ed., "The Dynamic Behavior of Liquids in Moving Containers," NASA Office of Scientific and Technical Information SP-106, Washington, 1966.

2 Abramson, H. N., "Dynamic Behavior of Liquids in Moving Containers," *Applied Mechanics Reviews*, Vol. 16, No. 7, July 1963, pp. 501–506.

3 Cooper, R. M., "Dynamics of Liquids in Moving Containers," *ARS Journal*, Vol. 30, Aug. 1960, p. 725.

4 Neu, J. T., and Good, R. J., "Equilibrium Behavior of Fluids in Containers at Zero-Gravity," *AIAA Journal*, Vol. 1, No. 4, Apr. 1963, pp. 814–819.

5 Satterlee, H. M., and Chin, J. H., "Meniscus Shape Under Reduced-Gravity Conditions," Symposium on Fluid Mechanics and Heat Transfer Under Low Gravitational Conditions, June 1965.

6 Hastings, L. J., and Rutherford, R., III, "Low Gravity Liquid-Vapor Interface Shapes in Axisymmetric Containers and a Computer Solution," NASA TM X-53790, Oct. 1968.

7 Petrash, D. A., and Otto, E. W., "Studies of the Liquid Vapor Interface Configuration in Weightlessness," ARS Space Power System Conference, Santa Monica, Calif., Paper No. 2514-62, 1962.

8 Satterlee, H. M., and Reynolds, W. C., "The Dynamics of the Free Liquid Surface in Cylindridal Containers Under Strong Capillary and Weak Gravity Conditions," TR LG-2, Department of Mechanical Engineering, Stanford University, May 1, 1964.

9 Yeh, G. C. K., "Free and Forced Oscillations of a Liquid in an Axisymmetric Tank at Low-Gravity Environments," JOURNAL OF APPLIED MECHANICS, Vol. 34, No. 1, TRANS. ASME, Vol. 89, Series E, Mar. 1967, pp. 23–28.

10 Dodge, F. T., and Garza, L. R., "Experimental and Theoretical Studies of Liquid Sloshing at Simulated Low Gravities," Technical Report No. 2, Contract No. NAS8-20290, Control No. DCN 1-6-75-00010, SwRI Project 02-1846, Southwest Research Institute, Oct. 1966; see also JOURNAL OF APPLIED MECHANICS, Vol. 34, No. 3, TRANS. ASME, Vol. 89, Series E, Sept. 1967, pp. 555–562.

11 Dodge, F. T., and Garza, L. R., "Simulated Low-Gravity Sloshing in a Cylindrical Tank Including Effects of Damping and Small Liquid Depth," *Proceedings, 1968 Heat Transfer and Fluid Mechanics Institute*, Stanford University Press, 1968, pp. 67–69.

12 Dodge, F. T., and Garza, L. R., "Simulated Low-Gravity Sloshing in Spherical Tanks and Cylindrical Tanks With Inverted Ellipsoidal Bottoms," Technical Report No. 6, Contract NAS8-20290, Control No. DCN 1-6-75-00010, SwRI Project No. 02-1846, Southwest Research Institute, Feb. 1968.

13 Dodge, F. T., and Garza, L. R., "Slosh Force, Natural Frequency, and Damping of Low-Gravity Sloshing in Oblated Ellipsoidal Tanks," Technical Report No. 7, Contract No. NAS8-20290, Control No. DCN 8-75-00043(IF), SwRI Project No. 02-1846, Southwest Research Institute, Feb. 1969.

14 Concus, P., Crane, G. E., and Satterlee, H. M., "Low Gravity Lateral Sloshing in Hemispherically Bottomed Cylindrical Tanks," *Proceedings, 1968 Heat Transfer and Fluid Mechanics Institute*, Stanford University Press, 1968, pp. 80–97.

15 Concus, P., Crane, G. E., and Satterlee, H. M., "Small Amplitude Lateral Sloshing in Spheroidal Containers Under Low Gravity Conditions," NASA CR-72500, LMSC-A944673, Lockheed Missiles and Space Co., Sunnyvale, Calif., February 4, 1969.

16 Chu, W. H., "Low Gravity Liquid Sloshing in an Arbitrary Asixymmetric Tank Performing Translational Oscillations," Technical Report No. 4, Contact No. NAS8-20290, Control No. DCN 1-6-75 00010, SwRI Project No. 02-1846, Southwest Research Institute, Mar. 1967.

17 Winslow, A. M., "Numerical Solutions of the Quasilinear Poison Equations in a Nonuniform Triangular Mesh," *Journal of Computational Physics*, Vol. 1, No. 2, Nov. 1966, pp. 149–172.

18 Wang, C. T., *Applied Elasticity*, McGraw-Hill, New York, 1953.

19 Sokolnikoff, I. S., *Mathematical Theory of Elasticity*, 2nd ed. McGraw-Hill, New York, 1956.

20 Abramson, H. N., Chu, W. H., and Ransleben, G. E., Jr., "Representation of Fuel Sloshing in Cylindrical Tanks by an Equivalent Mechanical Model," *ARS Journal*, Dec. 1961, pp. 1697–1705.

APPENDIX A

Brief Description of a Computer Program

The following steps of a computer program are briefly described.

Construction of a Triangular Mesh. The triangular mesh is generated as described in reference [17] except that a simple parallelogram is used as the logical diagram, Fig. 3. For a cylindrical tank at Bond number 100, the physical diagram is shown in Fig.

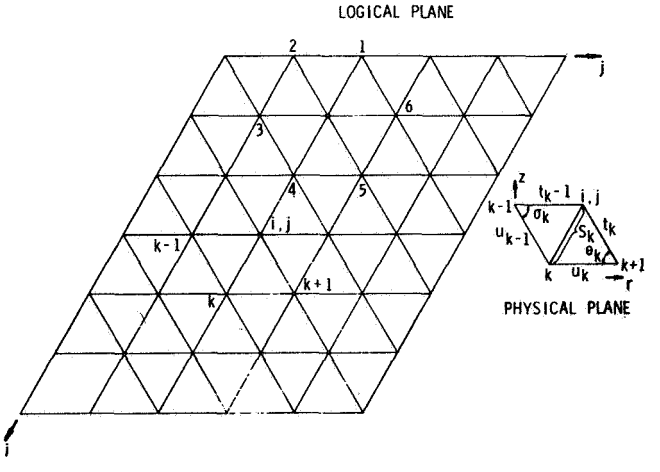

Fig. 3 Simple logical diagram for triangular mesh

4(*a*). For a spheroidal tank ($e = 0.5$) at Bond number 5, a triangular mesh is shown in Fig. 4(*b*). The lengths of the edge of the parallelogram can be adjusted for each individual case to yield desired triangular meshes. A continuous wall needs to be broken into two parts for the logical diagram. This only affects the local distribution of the triangular mesh and has shown to yield good results for a spheroidal tank, as well as a cylindrical tank.

Construction of Auxiliary Characteristic Functions. The characteristic functions ψ satisfy

$$\nabla^2\psi = 0 \tag{32}$$

$$\frac{\partial\psi}{\partial n_0} = 0 \quad \text{on } W \tag{33}$$

$$\frac{\partial\psi}{\partial n_0} = \lambda\psi \quad \text{on } F \tag{34}$$

ψ can be solved numerically with the constructed triangular mesh by Winslow method [17]. Contact point is treated as one of the mesh points, as are the other boundary points.[16] Hence, $\partial\psi/\partial n$ may be discontinuous at the contact point. Zero contact angle cannot be constructed graphically but results of decrease mesh size give closer and closer approximations to the interface and would probably lead to the correct limiting value.

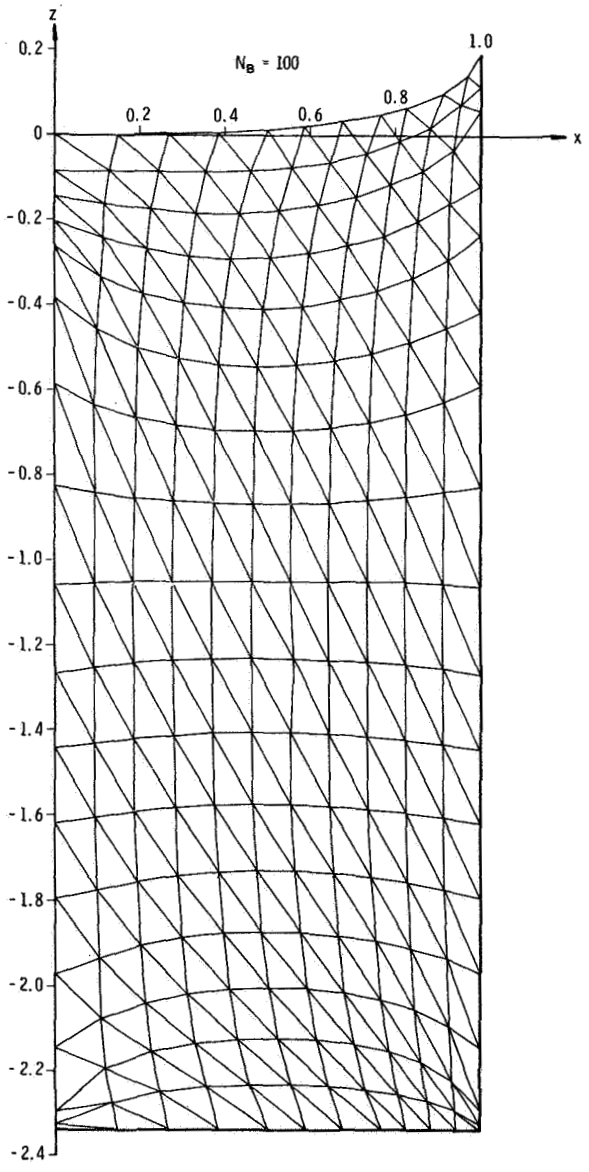

Fig. 4(a) Physical diagram of triangular mesh—cylindrical tank

For an interior joint, ij, [$\psi = \psi_{ij}$, $\psi_k = \psi_k(i, j)$, $r_k = r_k(i, j)$, $r = r_{ij}$]

$$\sum_{k=1}^{6} \omega_k(\psi_k - \psi) - \frac{m^2}{r_{ij}} A_{ij}\psi = 0 \tag{35}$$

where

A_{ij} = area of the ijth dodecagon [17] inside the fluid domain
r_{ij} = radius of the ijth point

$$\omega_k = \tfrac{1}{2}(\lambda_k \bar{r}_k \cot\theta_k + \lambda_{k-1}\bar{r}_{k-1}\cot\sigma_k) \quad k = 1 \text{ to } 6 \tag{35a}[17]$$

$$\bar{r}_k = \tfrac{1}{3}(r_{ij} + r_k + r_{k+1}) \quad \lambda_k = 1 \tag{35b, c}$$

θ_k, σ_k, Fig. 3, can be expressed in terms of t_k, u_{k+1}, t_{k-1}, u_{k-1}, and s_k.

For interface point,

$$\sum_{k=1}^{6} \omega_k(\psi_k - \psi) - \frac{m^2}{r_{ij}} A_{ij}\psi + \left(\frac{\partial\psi}{\partial n}\right)_{1,j}\left[\frac{1}{2}s_3 + \frac{1}{2}s_6\right] r_{ij} = 0 \tag{36}$$

where

$$\lambda_6 = \lambda_1 = \lambda_2 = 0, \quad \lambda_3 = \lambda_4 = \lambda_5 = 1$$

To solve for the eigenfunctions on the interface, we use the influence coefficient method in which $(\partial\psi/\partial n)_{1,i} = 0$ except $(\partial\psi/\partial n)_{1,j} = 1$ for the jth column of the influence matrix. A standard eigenvalue problem involving only the interface points, excluding $\psi_{1,1}$ at $r = 0$, is needed to obtain the eigenvalues λ_j and eigenvectors ψ_j. Knowing the jth eigenvector on the interface, the corresponding value of ψ_j on the wall can be easily solved numerically again by the method of overrelaxation.

For ijth point on the tank wall

$$\sum_{k=1}^{6} \omega_k(\psi_k - \psi) - \frac{m^2}{r_{ij}} A_{ij}\psi = 0 \tag{37}$$

$\lambda_3 = \lambda_4 = \lambda_5 = 0$ and $\lambda_1 = \lambda_2 = \lambda_6 = 1$ on the bottom wall

$\lambda_4 = \lambda_5 = \lambda_6 = 0$ and $\lambda_1 = \lambda_2 = \lambda_3 = 1$ on the side wall

On center line, $r = 0$,

$$\psi = 0 \text{ for } m \geq 1$$
$$\frac{\partial\psi}{\partial r} = 0 \text{ for } m = 0 \tag{38}$$

$$\lambda_1 = \lambda_2 = \lambda_3 = 0 \text{ and } \lambda_4 = \lambda_5 = \lambda_6 = 1$$

At contact point $i = 1, j = j_{mx}$.

$$\sum_{k=1}^{6} \omega_k(\psi_k - \psi) - \frac{m^2}{r_{ij}} A_{ij}\psi + \left(\frac{\partial\psi}{\partial n}\right)_{1,j_{mx}}\left(\frac{1}{2}s_3\right) r_{ij} = 0 \tag{39}$$

$$\lambda_3 = 1, \lambda_1 = \lambda_2 = \lambda_4 = \lambda_5 = \lambda_6 = 0$$

Calculation of Interface Shape. A program based on the theory of reference [6] was written to generate the interface shape with desired net points for a given empty fraction or central depth and a

[16] This represents conservation of mass in the triangle containing contact point. Experience shows that the contact point condition should not be imposed on ψ_j.

[17] Note: $(\lambda_{j-1/2})$ reference [17] $= \lambda_{j-1}$, $(\lambda_{j+1/2})$ reference [17] $= \lambda_j$.

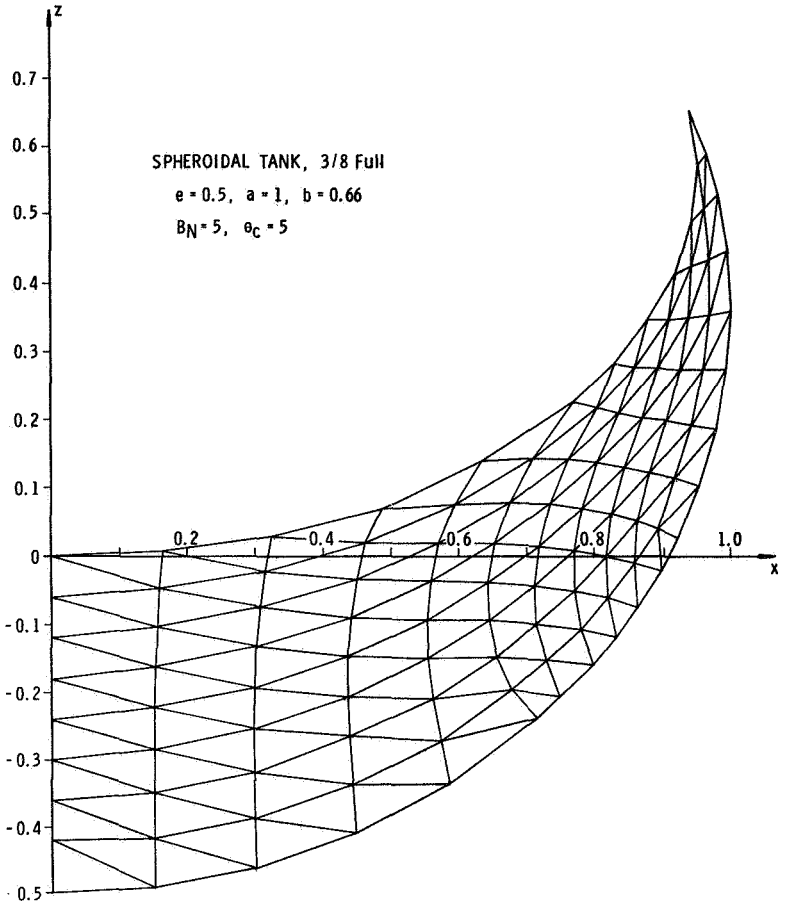

Fig. 4(b) Triangular mesh for spheroidal tank at low gravity

given contact angle. This program also calculates contact point constant Γ but limits the contact angle to possibly 2 deg or greater.

Calculation of Natural Frequencies, Slosh Masses, and Their Location

The remaining steps are relatively routine and, therefore, will not be described. It is, however, remarked that trapezoidal rule and midpoint rules were employed conveniently in evaluating the integrals. For some quantities, quadratic fittings were made, such as dF/dR, before entering the quadrature formulas.

APPENDIX B

A Modified Galerkin Method

In the Galerkin method, it is generally assumed [19] that each of the coordinate functions of a complete set satisfies the same boundary conditions as the exact solution. This condition seems to be a sufficient condition rather than a necessary condition since the series expansion as a whole may satisfy the prescribed conditions, not necessarily term by term. Since the solution, if continuous, can be expanded into a convergent series containing the complete set, the failure of the error minimization process, if it occurs, must lie in the insufficient differentiability of the series. Therefore, the present method as applied to a second-order ordinary differential equation performs integration by part, then imposes the remaining boundary condition[18] as illustrated by the following example.

Let y be governed by the simple equation

$$\frac{d^2y}{dx^2} + \lambda^2 y = 0; \qquad \lambda \neq \frac{2m-1}{2}\pi \tag{40}$$

subject to

$$y = 0 \qquad \text{at } x = 0 \tag{41}$$

$$\frac{dy}{dx} = \Gamma_1 \qquad \text{at } x = 1 \tag{42}$$

We shall select a complete set in (0, 1) which satisfies $y = 0$ at $x = 0$ but $y \neq 0$ at $x = 1$. To be specific, we express

$$y = \sum_{m=1}^{\infty} C_m \sin(\lambda_m x) \tag{43}$$

where

$$\lambda_m = \frac{2m-1}{2}\pi$$

Then, the modified Galerkin procedure minimizes the error of the differential equation as follows:

$$0 = \int_0^1 \sin(\lambda_n x)\left[\frac{d^2y}{dx^2} + \lambda^2 y\right] dx$$

$$= \left[\sin(\lambda_n x)\frac{dy}{dx}\right]_0^1 - \int_0^1 \lambda_n \frac{dy}{dx}\cos(\lambda_n x)dx$$

$$+ \int_0^1 \lambda^2 y \sin(\lambda_n x)dx = (-1)^{n-1}\Gamma_1$$

$$- \int_0^1 \lambda_n \lambda_m \sum_{m=1}^{\infty} C_m \cos(\lambda_n x)\cos(\lambda_m x)dx$$

[18] This may be a new technique to satisfy the boundary condition or conditions. However, a general proof and extension remain to be done.

$$+ \int_0^1 \lambda^2 \sum_{m=1}^{\infty} C_m \sin(\lambda_n x) \sin(\lambda_m x) dx$$

$$= (-1)^{n-1}\Gamma_1 - \left(\frac{\lambda_n^2}{2} - \frac{\lambda^2}{2}\right) C_n, \qquad n = 1, 2, \ldots, \infty \quad (44)$$

Thus

$$C_n = \frac{2\Gamma_1(-1)^{n-1}}{(\lambda_n^2 - \lambda^2)} \quad (45)$$

The exact solution of the problem is

$$y = \frac{\Gamma_1}{\lambda \cos \lambda} \sin(\lambda x) = \sum_{n=1}^{\infty} C_n' \sin(\lambda_n x) \quad (46)$$

It is easy to show that the Fourier coefficient C_n' of the exact solution is equal to C_n; thus the modified Galerkin method yields the exact solution in the limit.

The rate of convergence of the foregoing example ($\Gamma_1 \neq 0$) is only $1/n^2$ near the end, $x = 1$. This could be expected as dy/dx is zero term by term while with infinite terms converge to Γ_1 as a whole when $x \to 1$. Equation (13) in the text is analogously derived; however, the rate of convergence might be better as illustrated by results in Appendix III. It should be pointed out that at the high Bond numbers, each auxiliary characteristic function is a normal mode and, as Bond number decreases, more characteristic functions are required to represent each mode. Only by actual computation is one to find out how many of them are sufficient for engineering purposes.

APPENDIX C

Constant Contact Angle Condition

For small perturbed motions at the instantaneous contact point, Part 2, Fig. 5.

$$\theta_2 = \theta_1 + \beta \quad (47)$$

$$= \theta_0 + \left(\frac{\partial \theta_0}{\partial s}\right)_{II} dS_F + \left(\frac{\partial h}{\partial s}\right)_{II} \quad (48)$$

With $\tan \theta_0 = \frac{df}{dr}$, $\frac{dr}{ds} = \frac{\epsilon_1}{\sqrt{1 + f_r^2}}$, $\epsilon_1 = \operatorname{sgn}\left(\frac{dr}{df}\right)$, one has

$$\left(\frac{\partial \theta_0}{\partial s}\right)_{II} = \sec^2 \theta_0 \left(\frac{d^2 f}{dr^2} \frac{\epsilon_1}{\sqrt{1 + f_r^2}}\right)_{II} = \left[\frac{f_{rr}\epsilon_1}{(1 + f_r^2)^{3/2}}\right]_{II} \quad (49)$$

Similarly, at the instantaneous contact point 2,

$$\theta_{W_2} = \theta_{WII} + \left(\frac{\partial \theta_W}{\partial s_W}\right)_{II} ds_W \quad (50)$$

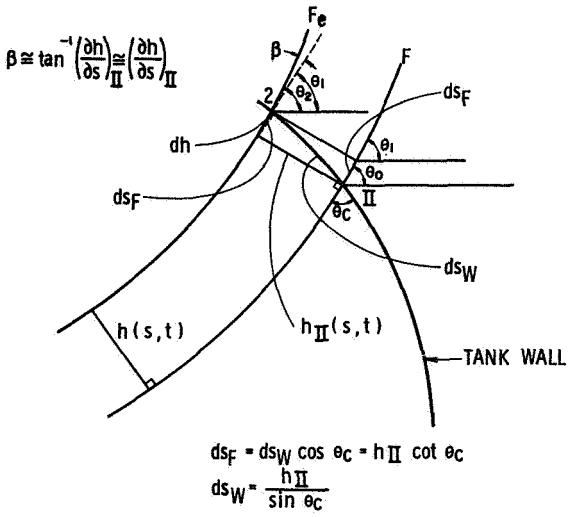

$$ds_F = ds_W \cos \theta_C = h_{II} \cot \theta_C$$

$$ds_W = \frac{h_{II}}{\sin \theta_C}$$

Fig. 5 Geometry for contact point condition

$$= \theta_{WII} + \left[\frac{z_{rr}\epsilon_2}{(1 + z_r^2)^{3/2}}\right]_{W,II} ds_W \quad (51)$$

where

$$\epsilon_2 = \operatorname{sgn}\left(\frac{dz}{dr}\right)$$

We shall assume constant contact angle independent of time t, i.e.,

$$\theta_c = \theta_{WII} - \theta_0 = \theta_{W_2} - \theta_2 = \text{const} \quad (52)$$

then, with $dS_W = \frac{h}{\sin \theta_c}$, $dS_F = dS_W \cos \theta_c$, Fig. 6.

$$\frac{f_{rr}\epsilon_1}{[1 + f_r^2]^{3/2}} \cos \theta_c \frac{h}{\sin \theta_c} + \frac{\partial h}{\partial s} - \frac{z_{RR}\epsilon_2}{[1 + z_R^2]^{3/2}} \frac{h}{\sin \theta_c} = 0 \quad \text{at II} \quad (53)$$

i.e.,

$$\frac{\partial h}{\partial s} = \gamma h \quad (54)$$

where

$$\gamma = \frac{1}{\sin \theta_c}\left[\frac{z_{rr}\epsilon_2}{(1 + z_r^2)^{3/2}} - \cos \theta_c \frac{f_{rr}\epsilon_1}{(1 + f_r^2)^{3/2}}\right]_{II} \quad (55)$$

For a convex tank with convex interface

$$\gamma = \frac{1}{\sin \theta_c}\left\{\left|\frac{z_{rr}}{(1 + z_r^2)^{3/2}}\right|_{W,II} - \cos \theta_c \left|\frac{f}{(1 + f_r^2)^{3/2}}\right|_{II}\right\} \quad (56)$$

APPENDIX D. NUMERICAL EXAMPLES

A. Flat Interface with High Bond Number in a Cylindrical Tank $N_B = 1000$, $\frac{h_o}{a} = 2.34$, $a = 0.68$ with $\Gamma = 0$, a 12×18 mesh yielded $\frac{\omega_1^2 a}{g} = 1.85$ compared with 1.847 from exact theory (Ref. 1 of Appendix B).

$\frac{m_1}{m_F} = 0.193$ compared with 0.194 from high-G theory (Ref. 19 of Appendix B).

$z_1 = -0.729$ in. compared with -0.724 in. from high-G theory (Ref. 19 of Appendix B).

B. Flat Interface with Low Bond Number in a Cylindrical Tank $N_B = 10$, $\frac{h_o}{a} = 2.34$, $a = 0.68$ with $\Gamma = 0$, 12×18 mesh yielded $\frac{\omega_1^2 a}{g} = 2.15$ compared with 2.46 from exact theory. A finer mesh is required for better agreement.

C. Curved Interface with Low Bond Number $N_B = 100$, $\frac{h_o}{a} = 2.34$, $a = 0.68$, $\theta_c = 2°$ yielded $\frac{\omega_1^2 a}{g} = 1.860$, $\frac{m_1}{\rho a^3} = 0.442$, $z_1 \cong -0.724$ in. compared with theoretical value of $\frac{\omega_1^2 a}{g} = 1.777$, $\frac{m_1}{\rho a^3} = 0.438$, $z_1 \cong -0.73$ in. (Ref. 12 of Appendix B). It is noted that experimental value of $\frac{\omega_1^2 a}{g}$ for $\theta_c = 0°$ is around 1.78 to 1.80. Finer net may lead to better approximation.

D. Spherical Tank with Flat Interface $N_B = 1000$, $\frac{h_o}{a} = 1$, $a = 1$ with $\Gamma = 0$, 11×11 mesh yielded $\frac{\omega_1^2 a}{g} = 1.54$ compared with high-G sloshing value of $\frac{\omega_1^2 a}{g} = 1.54$.

E. Spherical Tank with "Folding" Interface $N_B = 10$, $\frac{h_o}{a} \cong 1.14$*, $a = 1$, $\theta_c = 4.96°$ ($\Gamma = -65.788$), 12×12 mesh yield $\frac{\omega_1^2 a}{g} = 1.469$, $\frac{m_1}{\rho a^3} = 0.604$, $z_1 = -0.742$ in. compared with Lockheed result (Ref. 16 of Appendix B) of $\frac{\omega_1^2 a}{g} = 1.507$ (for $\theta_c = 5°$). The first slosh mass is much larger than that of Lockheed, probably due to the inclusion of force directly attributed to surface tension in the present theory which yielded confirmed results for cylindrical tanks (Case 3). The value of z_1 would be the location of the center of the sphere if the contribution due to direct surface tension [i.e., the integral over F in Eq. (30b)] is neglected.

F. Spheroidal Tank with Folding Interface Ellipticity $e = 0.5$, major axis $a = 1$, minor axis $b = 0.866$, $N_B = 5$, $\beta = 0.6263$ (3/8 full tank), $\frac{h_o}{a} \cong 0.4999$, $\theta_c = 5.06°$, ($\Gamma = -38.430$, $V_L = 1.35$).† 12×9 mesh (non-uniform on free surface) yielded $\frac{\omega_1^2 a}{g} = 1.114$‡, $\frac{m_1}{\rho V_L} = 0.582$, $z_1 = -0.5841$ compared with Lockheed result of $\frac{\omega_1^2 a}{g} = 0.966$. It is noted that the value of z_1 puts the first mass under the tank bottom which should be examined by future experiments when available.

*Calculated for 3/4-full tank.

†For $\theta_c = 5.06°$, the Γ used in ASME paper APM-EEE was in error and the correct value is given here as are the results.

‡With 23×17 mesh, $\frac{\omega_1^2 a}{a} = 1.079$, $\frac{m_1}{\rho V_L} = 0.5736$, $z_1 = -0.4644$; and $\frac{\omega_2^2 a}{g} = 15.03$ while Lockheed's result for $\frac{\omega_2^2 a}{g}$ is 13.26. It is uncertain which results are more accurate. The value of Γ has not been given by Lockheed to facilitate the explanation of the differences.